Biosensors

International Edition: DOI: 10.1002/anie.201911799
German Edition: DOI: 10.1002/ange.201911799

Genetically Encoded Ratiometric RNA-Based Sensors for Quantitative Imaging of Small Molecules in Living Cells

*Rigumula Wu, Aruni P. K. K. Karunanayake Mudiyanselage, Fatemeh Shafiei, Bin Zhao, Yousef Bagheri, Qikun Yu, Kathleen McAuliffe, Kewei Ren, and Mingxu You**

Abstract: *Precisely determining the intracellular concentrations of metabolites and signaling molecules is critical in studying cell biology. Fluorogenic RNA-based sensors have emerged to detect various targets in living cells. However, it is still challenging to apply these genetically encoded sensors to quantify the cellular concentrations and distributions of targets. Herein, using a pair of orthogonal fluorogenic RNA aptamers, DNB and Broccoli, we engineered a modular sensor system to apply the DNB-to-Broccoli fluorescence ratio to quantify the cell-to-cell variations of target concentrations. These ratiometric sensors can be broadly applied for live-cell imaging and quantification of metabolites, signaling molecules, and other synthetic compounds.*

Fluorescent probes that allow live-cell imaging of small molecules have enabled us to better understand cellular signaling and metabolite flux. Various fluorescent small-molecule probes and genetically encoded fluorescent protein (FP)-based sensors have been developed to image metabolites and signaling molecules.[1] The function of FP sensors requires a target-binding domain that can both selectively recognize the target and result in sufficient conformational change to refold the FP or change the orientation between two FPs.[2] However, for many physiologically important analytes, these adequate target-binding domains are not easily identified. The limited signal-to-noise ratio has further prevented their wide applications.[3]

We and others have developed a new class of genetically encoded sensors based on fluorogenic RNA aptamers.[4] Aptamers are short single-stranded oligonucleotides that can bind to their targets with high affinity and specificity.[5] Fluorogenic RNA aptamers, for example, Spinach or Broccoli, can bind and activate the fluorescence of dyes such as 3,5-difluoro-4-hydroxybenzylidene-1-trifluoroethyl-imidazolinone (DFHBI-1T).[6] By fusing a target-binding aptamer into Spinach/Broccoli, genetically encoded RNA-based sensors have been developed for live-cell imaging of metabolites, signaling molecules, proteins, and metal ions.[4,7]

Almost all these fluorogenic RNA sensors were developed based on a Spinach/Broccoli-dye complex ($\lambda_{ex}/\lambda_{em}$, approximately 480 nm/ 503 nm). With a single-wavelength readout, artifacts can easily arise from variations in the cellular RNA distributions. For quantitative and multiplexed imaging of cellular analytes,[8] it is critical to develop new RNA sensor pairs that have little spectra overlap and that can be orthogonally imaged.

Here, we develop ratiometric RNA sensors to quantify the cellular concentrations and distributions of small molecules. The sensor comprises Broccoli and a dinitroaniline (DN)-binding aptamer, DNB.[6b,9] We have engineered novel red-colored RNA sensors by fusing target-binding aptamers into DNB. Using Broccoli as the reference, we can quantitatively image various small molecules in living cells.

We first wondered if it is possible to develop DNB-based metabolite sensors. Dinitroaniline is a general contact quencher for fluorophores including sulforhodamine B (SR). The conjugation of DN and SR generates a non-fluorescent complex, SR-DN. The binding of DNB isolates DN, which activates the SR fluorescence.[9] After analyzing the DNB structure, we realized that its P4/L4 hairpin could be potentially used to fuse with target-binding aptamers (Figure 1 a).[9] We replaced this domain with three sequences that maintained a similar hairpin structure (Supporting Information, Figure S1). Similar to DNB (83.1-fold), all three mutations activated the SR-DN fluorescence (62.8- to 80.4-fold). In contrast, RNA with a mismatched P4 stem completely lost its binding with SR-DN (Supporting Information, Figure S1). Indeed, DNB functions depend on the structure, but not the sequence, of P4/L4.

We inserted an adenine-binding aptamer[10] into P4/L4 (Figure 1 a). In silico structural predication guided our design of five adenine-targeting sensors with different transducer sequences. An optimal sensor (Transducer 2, Supporting Information, Table S1) exhibited a 3.6-fold fluorescence enhancement in the presence of 10 μM adenine (Figure 1 b). Similarly, we developed DNB-based sensors for an antibiotic, tetracycline, and a signaling molecule, c-di-GMP.[4d,11] A 1.5- to 11.9-fold fluorescence increase was observed after adding 200 μM tetracycline (Figure 1 b). Interestingly, the optimal transducer sequence, Transducer 3, has been previously used in a ribozyme-based tetracycline sensor.[11a] An optimal sensor for c-di-GMP was achieved with a 10.6-fold fluorescence enhancement after adding 10 μM c-di-GMP. Transducer 1, whose sequence was previously used in a Spinach-based sensor c-di-GMP,[4d] also exhibited similar fold enhancement (Figure 1 b). Previously identified transducers may be directly applicable in these modular DNB-based sensors.

These sensors also preserve the high selectivity towards their targets (Figure 1 c). After demonstrating the robust sensor performance under different temperature and Mg^{2+}

[*] R. Wu, A. P. K. K. Karunanayake Mudiyanselage, F. Shafiei, Dr. B. Zhao, Y. Bagheri, Q. Yu, K. McAuliffe, Dr. K. Ren, Prof. M. You
University of Massachusetts, Amherst, MA 01003 (USA)
E-mail: mingxuyou@umass.edu
Supporting information and the ORCID identification number(s) for the author(s) of this article can be found under: https://doi.org/10.1002/anie.201911799.

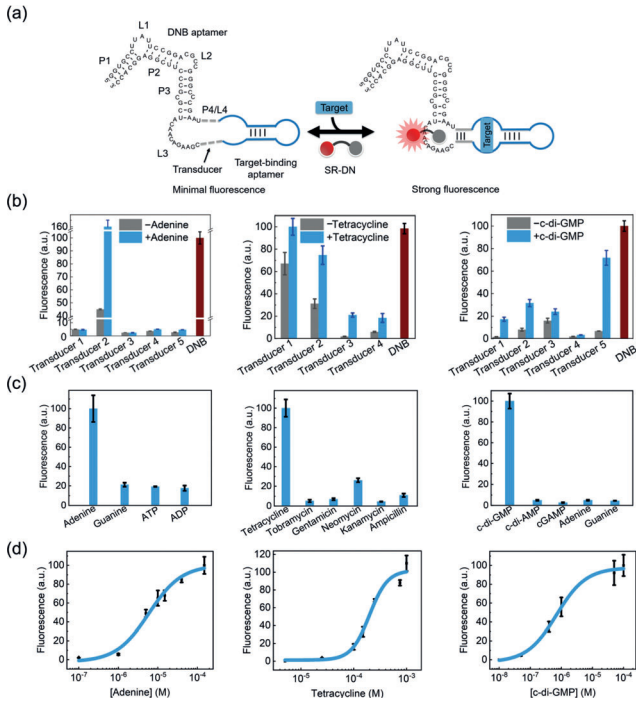

Figure 1. Design and in vitro characterization of DNB-based sensors. a) Schematic of DNB-based sensors, which comprise a target-binding aptamer (blue), a transducer (dashed gray), and DNB. Target binding induces the folding of transducer and DNB to activate the fluorescence of sulforhodamine B (SR). b) Optimization of transducers for DNB-based adenine, tetracycline, and c-di-GMP sensors. Fluorescence was measured with 5 μM RNA and 0.5 μM SR-DN at λ_{ex} = 571 nm and λ_{em} = 591 nm after incubating with 10 μM adenine, 200 μM tetracycline, or 10 μM c-di-GMP. c) Selectivity was measured in the presence of 10 μM, 1 mM, and 100 μM of the indicated compounds for adenine, tetracycline, and c-di-GMP sensors, respectively. d) Dose-response curve for fluorescence detection of targets by the optimal sensors. Shown are mean and SEM values of three independent replicates.

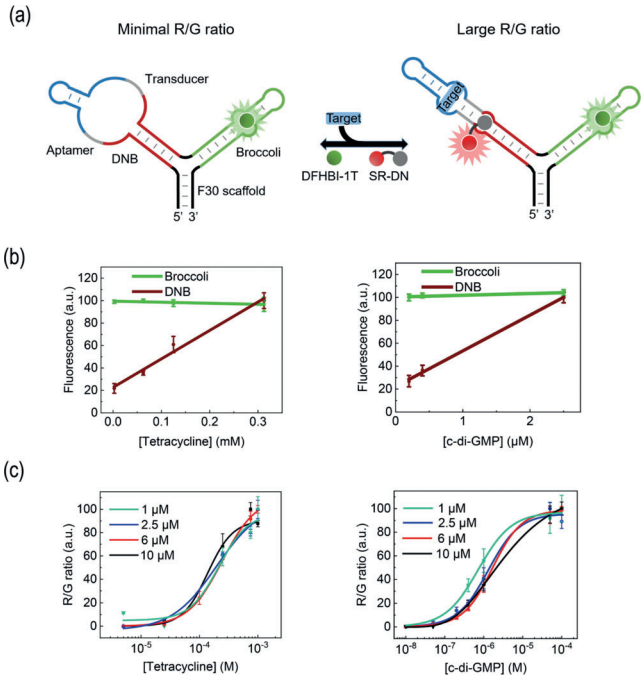

Figure 2. Design and in vitro characterization of ratiometric sensors. a) Schematic of the sensor that comprises an F30 scaffold (black), a Broccoli (green), and a DNB-based sensor. Target binding to the aptamer (blue) stabilizes the transducer duplex (gray), enabling DNB (red) to fold and activate the fluorescence of sulforhodamine B. b) Dose-response curves of the optimal ratiometric tetracycline and c-di-GMP sensors. Fluorescence was measured with 5 μM RNA and 0.5 μM SR-DN. c) Dose-response curves as measured at varying concentrations of RNA and 0.5 μM SR-DN. R/G ratio indicated the fluorescence ratio as measured at $\lambda_{ex}/\lambda_{em}$, 571 nm/ 591 nm (R) vs. that at λ_{ex}/y_{em}, 480 nm/ 503 nm (G). Shown are mean and SEM values of three independent replicates.

ion conditions (Supporting Information, Figure S2), we further studied their dynamic ranges (Figure 1d). The half-maximal fluorescence was reached after adding 5.9 μM adenine, 0.8 μM c-di-GMP, or 196 μM tetracycline. By defining the dynamic range as targets that induced 10–90% of maximum fluorescence, 1.0–40 μM adenine, 0.1–20 μM c-di-GMP, and 85–880 μM tetracycline could be detected. Indeed, these sensors could be potentially used to detect adenine (approximately 0.5–5 μM) and c-di-GMP (approximately 0.05–10 μM) in their physiological concentration ranges.[4d,12] The minimum antibacterial concentration of tetracycline is approximately 300 μM,[13] which is also suitable for detection with these DNB-based sensors.

We next asked if it is possible to use an RNA strand containing Broccoli ($\lambda_{ex}/\lambda_{em}$, 480 nm/ 503 nm) and DNB ($\lambda_{ex}/\lambda_{em}$, 571 nm/ 591 nm) to develop ratiometric sensors. To facilitate the proper folding of each aptamer, we inserted DNB and Broccoli into two arms of an F30 scaffold[14] (Figure 2a). After adding DFHBI-1T and SR-DN, both Broccoli/DFHBI-1T and DNB/SR-DN fluorescence could be easily detected and distinguished from each other (Supporting Information, Figure S3a,b). Thus, Broccoli and DNB can be used as an orthogonal fluorescent pair.

We wondered if ratiometric sensors (termed D/B) could be developed by conjugating DNB-based sensor with a Broccoli reference (Figure 2a). Indeed, a linear correlation was observed between the Broccoli fluorescence and RNA concentration (Supporting Information, Figure S3c). As expected, the Broccoli signal of D/B sensors remained constant after adding various amounts of targets, while the DNB fluorescence can be used to detect target concentrations (Figure 2b). Half-maximal fluorescence was reached with 122 μM tetracycline or 0.95 μM c-di-GMP, and a linear detection range of 1–250 μM and 0.2–2.5 μM was observed, respectively (Figure 2b). These D/B sensors still retained high selectivity towards the targets (Supporting Information, Figure S3f).

Alternative B/D sensors could be developed using a DNB reference and a Broccoli-based sensor (Supporting Information, Figure S4a). We first engineered a previously reported Broccoli-based c-di-GMP sensor[6b] into a ratiometric sensor. After adding different amounts of c-di-GMP, the DNB fluorescence was not influenced, while the Broccoli fluorescence was linearly correlated with c-di-GMP (Supporting Information, Figure S4c). Similarly, we developed another ratiometric B/D sensor for tetracycline. Using the same Transducer 3 from the DNB-based tetracycline sensor (Fig-

ure 1b), an optimal B/D sensor selectively responded to tetracycline with a linear detection range of 10–400 μM (Supporting Information, Figure S4d). Thus, using a DNB reference, we can potentially convert existing Broccoli-based sensors into sensors for ratiometric analysis.

We next asked if DNB and Broccoli fluorescence could be orthogonally imaged in living cells. We synthesized three plasmids expressing either F30-Broccoli, F30-DNB or both aptamers (F30-DNB/Broccoli) (Supporting Information, Figure S5). After transforming into *Escherichia coli*, the cellular fluorescence was imaged in the presence of DFHBI-1T and SR-DN. The Broccoli and DNB fluorescence could be clearly visualized in two separate channels without influencing each other (Figure 3a).

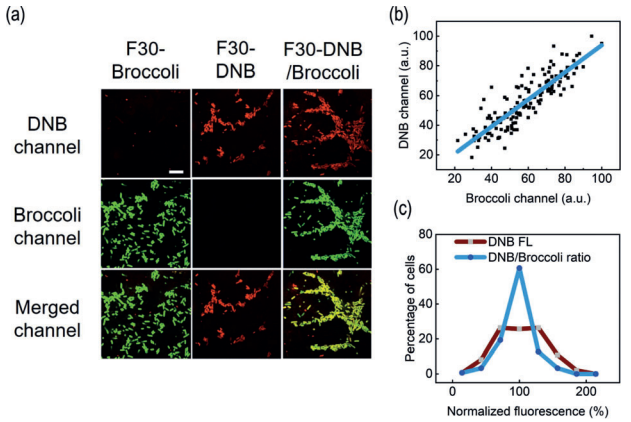

Figure 3. Orthogonal live-cell imaging of DNB and Broccoli. a) Fluorescence imaging of BL21 (DE3)* cells expressing F30-Broccoli, F30-DNB, or F30-DNB/Broccoli in the presence of 200 μM DFHBI-1T and 1 μM SR-DN. Scale bar, 10 μm. b) A linear correlation between DNB and Broccoli fluorescence in 150 cells expressing F30-DNB/Broccoli. Pearson's $r^2 = 0.8$. c) After analyzing 150 individual F30-DNB/Broccoli expressing cells, the distribution of DNB fluorescence levels was compared to that of DNB/Broccoli ratio.

We further analyzed individual cells that express F30-DNB/Broccoli, and, a linear correlation of Broccoli and DNB fluorescence was observed (Figure 3b). After comparing the cellular distributions of DNB fluorescence with that of DNB/Broccoli ratio (Figure 3c), indeed, a largely symmetric Gaussian distribution was shown only after ratiometric normalization. This is one demonstration of the importance of ratiometric imaging. We have further used real-time PCR to quantify the cellular F30-DNB/Broccoli RNA levels after different times of IPTG induction (Supporting Information, Figure S6). The cellular DNB-to-Broccoli fluorescence ratio is independent of RNA levels. The cellular fluorescence in both Broccoli and DNB channels were linearly correlated with the aptamer concentrations (Supporting Information, Figure S6). We can use either Broccoli or DNB as the reference to normalize sensor expression levels.

We next asked if we could apply D/B sensors to image and determine target levels in living cells. We first chose tetracycline-targeting Tc-D/B as an example. After adding 40–1000 μM tetracycline, target-dependent activation of DNB fluorescence was observed, while the Broccoli fluorescence remained at a constant level (Figure 4a). Our in vitro data indicated that independent of RNA concentration, the DNB-to-Broccoli fluorescence ratio could be directly correlated with target concentration (Figure 2c). A linear detection range of 70–750 μM for tetracycline and 0.3–10 μM for c-di-GMP was observed.

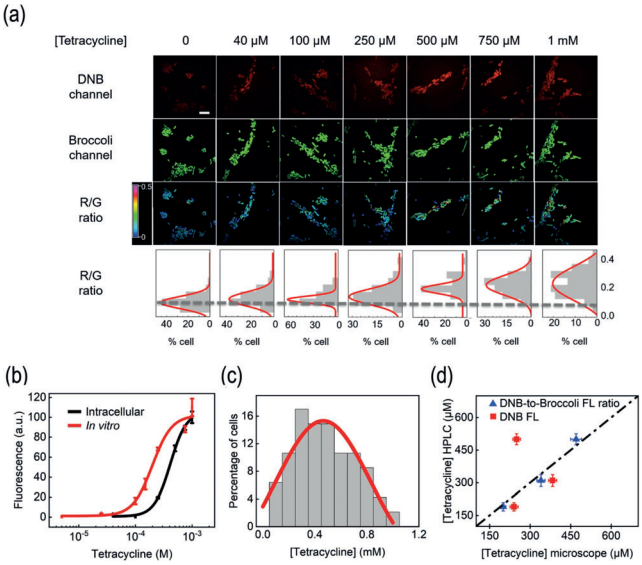

Figure 4. Intracellular imaging of tetracycline. a) Fluorescence imaging of BL21 (DE3)* cells expressing Tc-D/B after 70 min incubation with 0–1000 μM tetracycline. Scale bar, 10 μm. According to the DNB-to-Broccoli fluorescence (R/G) ratio of 300 individual cells from three experimental replicates, a distribution curve was generated. b) In vitro and cellular dose-response curves of Tc-D/B based on the mean and SEM DNB-to-Broccoli fluorescence ratio. c) Cellular distribution of tetracycline after adding 1 mM tetracycline. Individual cells were binned according to tetracycline concentration. The percentage of cells in each bin was plotted. d) Validation of the determined cellular tetracycline levels with an HPLC assay after adding 250, 500, and 1000 μM tetracycline. The tetracycline levels were determined based on either DNB fluorescence only (red) or DNB-to-Broccoli fluorescence ratio (blue).

We analyzed 300 individual cells at each tetracycline concentration (Figure 4a,b). On average a 1.6-fold, 2.7-fold, and 3.3-fold increase in the DNB-to-Broccoli fluorescence ratio was observed after adding 250, 500, and 1000 μM tetracycline, respectively (Figure 4b). Based on the calibration curve, these fluorescence ratios were correlated with 200, 340, and 470 μM cellular tetracycline, respectively (Figure 2c). The lower intracellular than extracellular tetracycline concentration is likely due to the reduced cell membrane permeability or the activation of efflux pumps.[15] We have further applied an HPLC assay[16] to validate the determined tetracycline concentrations (Supporting Information, Figure S7). Indeed, the determined values from the HPLC assay and fluorescence imaging matched each other well (Figure 4d).

We wondered if cellular tetracycline levels can be accurately determined by only measuring the DNB fluorescence. Based on the corresponding dose-responsive curve (Supporting Information, Figure S8) and Pearson correlation

coefficient (Supporting Information, Figure S9), the determined tetracycline levels with DNB-only images were quite different to those from ratiometric images. By comparing with the HPLC results (Figure 4d), ratiometric images quantified tetracycline levels with obvious higher accuracy, especially at high concentrations.

We further analyzed the cellular distributions of tetracycline. After adding 1 mM tetracycline, 18%, 50%, and 32% of cells accumulated high (greater than 650 μM), medium (300–650 μM), and low (less than 300 μM) levels of tetracycline (Figure 4c). To test if the cellular tetracycline accumulation is directly correlated with cell death, we used a Sytox Blue (SB) dye to stain the dead/dying cells (Supporting Information, Figure S10). The percentage of SB-stained cells increased from almost zero in the absence of tetracycline to 9.7%, 16%, and 30% after 2 h incubation with 40, 500, and 1000 μM tetracycline, respectively. SB-stained cells (90.3%) also exhibited high levels of tetracycline. Indeed, the intracellular accumulation of tetracycline is highly correlated with reduced cellular survival.

We further applied the c-di-GMP-targeting CDG-D/B sensor to image cellular c-di-GMP. It is known that the diguanylate cyclase GGDEF domain can be used to catalyze the synthesis of c-di-GMP.[17] Indeed, without GGDEF expression, the cellular DNB fluorescence was relatively low: 25.9%, 46.3%, and 27.8% of cells exhibited low (less than 0.2 μM), medium (0.2–10 μM), and high (greater than 10 μM) c-di-GMP levels (Figure 5a,c). After expressing GGDEF, bright DNB fluorescence was observed (Figure 5a), with 97.9% of cells exhibiting a high level (greater than 10 μM) of c-di-GMP (Figure 5b). Again, an HPLC assay[18] was used to validate the determined c-di-GMP concentrations (Supporting Information, Figure S11). After 1 h or 1.5 h IPTG induction, the calculated c-di-GMP level based on the cellular DNB-to-Broccoli fluorescence ratio was 13 μM and 7.3 μM, respectively. Quite similarly, the c-di-GMP level as determined in the HPLC assay was 11 μM and 7.1 μM, respectively, in these two conditions. While if only using DNB fluorescence for the calculation, a large variation from the HPLC results was observed, i.e., 20 μM and 16 μM, respectively (Supporting Information, Table S2). Indeed, D/B sensors could be used to quantify the cellular levels and distributions of signaling molecules.

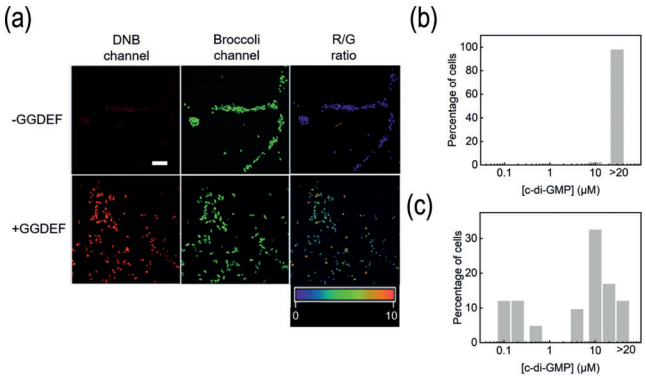

Figure 5. Quantitative imaging of c-di-GMP. a) Fluorescence imaging of c-di-GMP in live BL21 (DE3)* cells. 200 μM DFHBI-1T and 1 μM SR-DN were added 70 min before imaging. Scale bar, 10 μm. b,c) Cellular distribution of c-di-GMP in the presence (b) or absence (c) of GGDEF. Individual cells were binned according to c-di-GMP concentration. The percentage of cells in each bin was plotted.

In conclusion, we have developed ratiometric RNA-based sensors that can be modularly adapted to quantify various analyte levels in individual cells. Independent of RNA expression level, the cellular DNB-to-Broccoli fluorescence ratio can be used to quantify target concentrations. For the first time, red-colored fluorogenic RNA-based sensors have been developed for imaging small molecules. These new powerful genetically encoded sensors can be broadly applied for intracellular imaging of small molecules.

Acknowledgements

We acknowledge the support of start-up, NIH R01AI136789, T32GM008515, NSF CAREER, and Alfred P. Sloan Research Fellowship. We thank Dr. James Chambers for the assistance in fluorescence imaging, Dr. Kathryn Williams for revising the manuscript, and Drs. Craig Martin, S. Thayumanavan, Stephen Lory, and M. Sloan Siegrist for valuable comments.

Conflict of interest

The authors declare no conflict of interest.

Keywords: aptamers · biosensors · imaging agents · fluorogenic RNA · ratiometric sensors

[1] a) J. Zhang, R. E. Campbell, A. Y. Ting, R. Y. Tsien, *Nat. Rev. Mol. Cell Biol.* **2002**, *3*, 906–918; b) S. Okumoto, *Curr. Opin. Biotechnol.* **2010**, *21*, 45–54; c) Q. Ni, S. Mehta, J. Zhang, *FEBS J.* **2018**, *285*, 203–219; d) D. Liu, T. Evans, F. Z. Zhang, *Metab. Eng.* **2015**, *31*, 35–43; e) W. B. Frommer, M. W. Davidson, R. E. Campbell, *Chem. Soc. Rev.* **2009**, *38*, 2833–2841; f) A. Miyawaki, Y. Niino, *Mol. Cell* **2015**, *58*, 632–643.

[2] a) L. Lindenburg, M. Merkx, *Sensors Basel* **2014**, *14*, 11691–11713; b) A. Germond, H. Fujita, T. Ichimura, T. M. Watanabe, *Biophys. Rev.* **2016**, *8*, 121–138.

[3] a) A. Miyawaki, *Annu. Rev. Biochem.* **2011**, *80*, 357–373; b) A. E. Palmer, Y. Qin, J. G. Park, J. E. McCombs, *Trends Biotechnol.* **2011**, *29*, 144–152.

[4] a) J. S. Paige, T. Nguyen-Duc, W. J. Song, S. R. Jaffrey, *Science* **2012**, *335*, 1194–1194; b) W. J. Song, R. L. Strack, S. R. Jaffrey, *Nat. Methods* **2013**, *10*, 873–875; c) M. You, J. L. Litke, S. R. Jaffrey, *Proc. Natl. Acad. Sci. USA* **2015**, *112*, E2756–E2765; d) C. A. Kellenberger, S. C. Wilson, J. Sales-Lee, M. C. Hammond, *J. Am. Chem. Soc.* **2013**, *135*, 4906–4909; e) Q. Yu, J. Shi, A. P. K. K. Karunanayake Mudiyanselage, R. Wu, B. Zhao, M. Zhou, M. You, *Chem. Commun.* **2019**, *55*, 707–710; f) A. P. K. K. Karunanayake Mudiyanselage, R. Wu, M. A. Leon-Duque, K. Ren, M. You, *Methods* **2019**, *161*, 24–34; g) Z. M. Ying, Z. Wu, B. Tu, W. H. Tan, J. H. Jiang, *J. Am. Chem. Soc.* **2017**, *139*, 9779–9782; h) S. Sharma, A. Zaveri, S. S. Visweswariah, Y. Krishnan, *Small* **2014**, *10*, 4276–4280;

i) C. A. Kellenberger, S. C. Wilson, S. F. Hickey, T. L. Gonzalez, Y. Su, Z. F. Hallberg, T. F. Brewer, A. T. Iavarone, H. K. Carlson, Y. F. Hsieh, M. C. Hammond, *Proc. Natl. Acad. Sci. USA* **2015**, *112*, 5383 – 5388; j) M. D. E. Jepsen, S. M. Sparvath, T. B. Nielsen, A. H. Langvad, G. Grossi, K. V. Gothelf, E. S. Andersen, *Nat. Commun.* **2018**, *9*, 18.

[5] a) K. M. Song, S. Lee, C. Ban, *Sensors Basel* **2012**, *12*, 612 – 631; b) M. N. Stojanovic, D. M. Kolpashchikov, *J. Am. Chem. Soc.* **2004**, *126*, 9266 – 9270.

[6] a) J. S. Paige, K. Y. Wu, S. R. Jaffrey, *Science* **2011**, *333*, 642 – 646; b) G. S. Filonov, J. D. Moon, N. Svensen, S. R. Jaffrey, *J. Am. Chem. Soc.* **2014**, *136*, 16299 – 16308.

[7] Z. Sun, T. Nguyen, K. McAuliffe, M. You, *Nanomaterials Basel* **2019**, *9*, E233.

[8] a) Y. H. Chen, W. J. Liu, Z. M. Zhang, C. Zheng, Y. J. Huang, R. Z. Cao, D. Z. Zhu, L. Xu, M. Zhang, Y. H. Zhang, J. N. Fan, L. H. Jin, Y. K. Xu, C. F. Kuang, X. Liu, *Nat. Commun.* **2018**, *9*, 4818; b) S. Modi, M. G. Swetha, D. Goswami, G. D. Gupta, S. Mayor, Y. Krishnan, *Nat. Nanotechnol.* **2009**, *4*, 325 – 330.

[9] A. Arora, M. Sunbul, A. Jaschke, *Nucleic Acids Res.* **2015**, *43*, e144.

[10] M. Mandal, R. R. Breaker, *Nat. Struct. Mol. Biol.* **2004**, *11*, 29 – 35.

[11] a) A. Wittmann, B. Suess, *Mol. BioSyst.* **2011**, *7*, 2419 – 2427; b) X. C. Wang, S. C. Wilson, M. C. Hammond, *Nucleic Acids Res.* **2016**, *44*, e139.

[12] a) T. W. Traut, *Mol. Cell. Biochem.* **1994**, *140*, 1 – 22; b) R. Hengge, *Nat. Rev. Microbiol.* **2009**, *7*, 263 – 273; c) D. Kalia, G. Merey, S. Nakayama, Y. Zheng, J. Zhou, Y. Luo, M. Guo, B. T. Roembke, H. O. Sintim, *Chem. Soc. Rev.* **2013**, *42*, 305 – 341.

[13] C. F. Chang, L. C. Chang, Y. F. Chang, M. Chen, T. S. Chiang, *J. Vet. Diagn. Invest.* **2002**, *14*, 153 – 157.

[14] a) G. S. Filonov, C. W. Kam, W. J. Song, S. R. Jaffrey, *Chem. Biol.* **2015**, *22*, 649 – 660; b) G. S. Filonov, S. R. Jaffrey, *Curr. Protoc. Chem. Biol.* **2016**, *8*, 1 – 28.

[15] a) M. A. Webber, L. J. V. Piddock, *J. Antimicrob. Chemother.* **2003**, *51*, 9 – 11; b) K. L. May, M. Grabowicz, *Proc. Natl. Acad. Sci. USA* **2018**, *115*, 8852 – 8854.

[16] a) T. J. Franklin, *Biochem. J.* **1967**, *105*, 371 – 378; b) H. Yu, H. Mu, Y. M. Hu, *J. Pharm. Anal.* **2012**, *2*, 76 – 81.

[17] a) R. Simm, M. Morr, A. Kader, M. Nimtz, U. Romling, *Mol. Microbiol.* **2004**, *53*, 1123 – 1134; b) A. S. N. Seshasayee, G. M. Fraser, N. M. Luscombe, *Nucleic Acids Res.* **2010**, *38*, 5970 – 5981.

[18] A. B. Roy, O. E. Petrova, K. Sauer, *Bio-Protoc.* **2013**, *3*, e828.

Manuscript received: September 15, 2019
Accepted manuscript online: October 7, 2019
Version of record online: ■■ ■■, ■■■■

Communications

Biosensors

R. Wu,
A. P. K. K. Karunanayake Mudiyanselage,
F. Shafiei, B. Zhao, Y. Bagheri, Q. Yu,
K. McAuliffe, K. Ren,
M. You* ———— ■■■■–■■■■

Genetically Encoded Ratiometric RNA-Based Sensors for Quantitative Imaging of Small Molecules in Living Cells

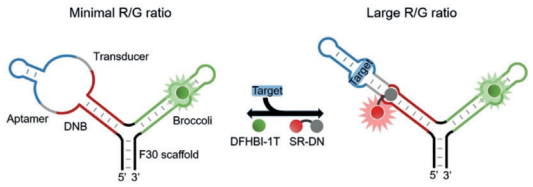

Ratiometric fluorogenic RNA-based sensors were developed to quantify metabolites and signaling molecules in living cells. Novel red-colored RNA-based sensors were engineered. These RNA-based sensors can be genetically encoded and engineered into versatile probes for a wide range of cellular targets.